New Phytologist

Research

Brassinosteroid signaling promotes sulfate uptake under sulfur deficiency in Arabidopsis

Xuanyi Chen, Zhenghao Yu, Wendi Guo, Yuting Zhou, Cun Wang and Tian Wang

State Key Laboratory for Crop Stress Resistance and High-Efficiency Production, College of Life Sciences, Northwest A&F University, Yangling, Shaanxi, 712100, China

Authors for correspondence:
Tian Wang
Email: tianwang2015@nwafu.edu.cn

Cun Wang
Email: cunwang@nwafu.edu.cn

Received: *24 February 2025*
Accepted: *25 June 2025*

New Phytologist (2025)
doi: 10.1111/nph.70390

Key words: Arabidopsis, brassinosteroid signaling, BZR1, sulfate transport, SULTR1;2.

Summary

- Sulfur (S) is a crucial macronutrient for plant growth, development, and stress tolerance. It serves as an essential component of amino acids (cysteine and methionine), vitamins, sulfatides, and coenzymes. S deficiency impairs plant productivity; yet, the molecular mechanisms regulating sulfate uptake remain poorly understood.
- In this study, brassinosteroid (BR) signaling was found to be activated under S deficiency, leading to the nuclear accumulation of BZR1, a central transcription factor in the BR signaling. BZR1 expression increased at both the mRNA and protein levels under S deficiency conditions.
- *SULTR1;2*, a high-affinity sulfate transporter, was identified as a direct downstream target of BZR1 through *in vitro* and *in vivo* analyses. Genetic and physiological evidence demonstrated that BZR1 promotes sulfate uptake via *SULTR1;2* in a BR-dependent manner.
- These findings uncover a molecular mechanism by which BR signaling regulates the S deficiency response through BZR1-mediated activation of *SULTR1;2*. This work enhances our understanding of nutrient signaling in Arabidopsis and provides potential targets for improving S use efficiency in crops.

Introduction

Sulfur (S) is an essential macronutrient in plants, which functions in plant growth, development, and stress tolerance (Fernández *et al.*, 2024). S is primarily absorbed from the soil in the form of sulfate ions (SO_4^{2-}) through plant roots to synthesize amino acids like cysteine and methionine as well as vitamins, sulfatides, and coenzymes (such as thiamine, biotin, and coenzyme A), which are crucial for both animals and humans (Ristova & Kopriva, 2022). Plants serve as a critical hub in the global S cycle, converting inorganic S into organic forms (Zhou *et al.*, 2025). However, recent studies have shown a significant decline in soil S deposition due to reduced SO_2 emissions in recent decades, raising concerns about potential S deficiencies in the future (Wang *et al.*, 2018; Aas *et al.*, 2019; Hinckley *et al.*, 2020).

The *sul*fate *t*ransporter (SULTR) system has four SULTR subgroups (SULTR1s–4s) (Takahashi, 2019). High-affinity SULTR1;1 and SULTR1;2, located in the roots, are primarily responsible for sulfate (SO_4^{2-}) uptake from soil (Takahashi *et al.*, 2000; Yoshimoto *et al.*, 2002). SULTR1;1 and SULTR1;2 have redundant functions in sulfate influx, whereas SULTR1;2 plays a dominant role (Yoshimoto *et al.*, 2007; Barberon *et al.*, 2008). SULTR1;2 is thought to be the potential sulfate sensor via its Anti-Sigma factor antagonist (STAS) domain (Shibagaki & Grossman, 2006). Once sulfate enters the root, SULTR2;1 and SULTR3;5 transfer the SO_4^{2-} from root to shoot (Takahashi *et al.*, 2000; Kataoka *et al.*, 2004a). SULTR1;3 functions in the loading of sulfate to the phloem (Yoshimoto *et al.*, 2003). SULTR3s and SULTR4s are involved in SO_4^{2-} influx from cytosol to chloroplast and efflux from vacuole to cytosol, respectively (Kataoka *et al.*, 2004b; Z. Chen *et al.*, 2019). The conversion of SO_4^{2-} into organic forms occurs in the chloroplast (Kataoka *et al.*, 2004b). The molecular functions of SULTRs are well understood, while the regulators controlling sulfate uptake are poorly understood (Takahashi, 2019; Fernández *et al.*, 2024). SILM1, a member of the ETHYLENE INSENSITIVE 3-LIKE transcription factor (TF) family, has been well characterized as the key regulator of sulfate uptake, assimilation, and S homeostasis under S deficiency conditions (Maruyama-Nakashita *et al.*, 2006; Aarabi *et al.*, 2016). Additionally, ELONGATED HYPOCOTYL 5 (HY5) has been identified to regulate sulfate uptake in response to S deficiency (Lee *et al.*, 2011).

Brassinosteroids (BRs) participate in almost the whole life of plants, from growth to development, including the response to various abiotic and biotic stresses (Planas-Riverola *et al.*, 2019; Nolan *et al.*, 2020; Han *et al.*, 2023). Over the past two decades, BR signaling has been well elucidated. BR signaling is initiated when BR molecules bind to their receptor BRASSINOSTEROID INSENSITIVE 1 (BRI1), a leucine-rich receptor kinase located on the plasma membrane (Li & Chory, 1997; She *et al.*, 2011). Upon activation, BRI1 phosphorylates the co-receptor BRI1-ASSOCIATED RECEPTOR KINASE 1 (BAK1) (Li *et al.*, 2002; Wang *et al.*, 2008). The BRI1–BAK1 complex functions as heterodimers (Nam & Li, 2002; Russinova

et al., 2004). This binding then leads to the dephosphorylation, ubiquitination, and degradation of BRASSINOSTEROID-INSENSITIVE2 (BIN2), resulting in protein phosphatase 2A (PP2A)-mediated dephosphorylation and nuclear accumulation of BRASSINAZOLE RESISTANT 1 (BZR1)/bri1-EMS-SUPPRESSOR 1 (BES1) family TFs, which mediate BR-responsive gene expression and plant growth (Li & Nam, 2002; Wang *et al.*, 2002; Yin *et al.*, 2002; He *et al.*, 2005; Kim *et al.*, 2009; Tang *et al.*, 2011). RNA-sequencing (RNA-seq) and Chromatin immunoprecipitation (ChIP)-sequencing (ChIP-seq) analyses have revealed that BZR1 and BES1 target regions enriched with the E-box motif (5′-*CANNTG*-3′) and the G-box motif (5′-*CACGTG*-3′) (Sun *et al.*, 2010; Yu *et al.*, 2011). Recent studies have shown that BR signaling can respond to the deficiency of nitrogen and phosphorus (Wang *et al.*, 2023b; Al-Mamun *et al.*, 2024; He *et al.*, 2024). Additionally, we noticed that several BR biosynthesis genes are upregulated under sulfate deficiency in the published transcriptome data (Yu *et al.*, 2022). Another study revealed that BZR1 participates in S metabolism (M. Wang *et al.*, 2023). However, the exact role of BR in the response to S deficiency and the underlying molecular mechanisms of BR-regulated sulfate uptake remain unclear.

In this study, we demonstrated that BR signaling positively regulates the response to S deficiency, mainly mediated by BZR1 in Arabidopsis. The response to S deficiency of BZR1 not only occurs at the translational level but also at the cellular, translational, and posttranslational levels. Through genetic and molecular approaches, we proved that sulfate transporter *SULTR1;2* is the direct target of BZR1. Furthermore, we employed the structure predictions and published epigenomic data to shed light on the molecular and structural mechanism underlying BR-responsive transcriptional regulation of S deficiency.

Materials and Methods

Plant materials and growth conditions

All *Arabidopsis thaliana* used in this research are Col-0 background except *bin2-3 bil1 bil2* (Ws background). The *bes1-D*, *bzr1-1D*, *BES1-RNAi* (#1, #2), *bes1-c2/bzr1-c1*, *pBZR1:BZR1-YFP*, *pBZR1:bzr1-1D-CFP*, *bin2-3 bil1 bil2*, *bri1-301*, *sultr1;1* (SALK_093256), and *sultr1;2* (SALK_122974) were used in this study (Wang *et al.*, 2002; Yin *et al.*, 2005; Xu *et al.*, 2008, 2021; Yan *et al.*, 2009; González-García *et al.*, 2011; Chaiwanon & Wang, 2015; Liang *et al.*, 2018; Tian *et al.*, 2018; W. Chen *et al.*, 2019; Yao *et al.*, 2022). Double mutant *bzr1-1D*/*sultr1;2* was obtained by crossing *bzr1-1D* and *sultr1;2*. Double mutant *sultr1;1*/*sultr1;2* was obtained by crossing *sultr1;1* and *sultr1;2*.

Arabidopsis plants were grown at 22°C : 20°C under 16 h : 8 h, light : dark cycles. For phenotypic analysis, the seeds were sterilized with 70% sodium hypochlorite (NaClO) containing 0.025% Triton X-100, followed by washing with ddH_2O seven times. For preparation of agar medium, agar was washed seven times with 1 l of ddH_2O. The pH of the medium was adjusted to 5.80 in this article. The S sufficiency medium (+Sul) was based on a half-strength Murashige and Skoog medium (½MS) (PhytoTech Labs, Lenexa, KS, USA) containing 1% sucrose and 1% agar. The S deficiency medium (–Sul) was also based on ½MS, while all the sulfate was substituted with chloride (Coolaber, Beijing, China), containing 1% sucrose and 1% agar. Root length was measured by ImageJ.

For agar-based S deficiency conditions, seeds were germinated on +Sul medium for 4 d and then transferred to +Sul and –Sul agar medium for an additional 8 d. For hydroponic S deficiency conditions, seeds were germinated on +Sul medium for 5 d and subsequently transferred to either S1500 or S15 liquid medium for 2 wk. S1500 contained 1500 μM $MgSO_4$ as the sulfate source, whereas S15 contained 15 μM $MgSO_4$ and 1485 μM $MgCl_2$ to maintain ionic balance (Hirai *et al.*, 1995; Aarabi *et al.*, 2016). For S-free conditions, seeds were directly grown in +Sul and –Sul liquid medium for 8 d.

Measurements of chlorophyll content

The shoots were weighed and added to 95% ethyl alcohol, and then incubated overnight at room temperature. The absorbance of the samples was measured at wavelengths of 665, 649 nm to calculate Chl*a* and Chl*b* concentrations, respectively.

Measurement of anthocyanin contents

Anthocyanin contents were measured as previously described (Gao *et al.*, 2020). Briefly, Arabidopsis shoots were weighed and collected into 1 ml of anthocyanin extraction buffer (iso-propanol : HCl : water = 18 : 1 : 8). The samples were incubated overnight at room temperature away from light and then centrifuged at 12 000 × ***g*** for 10 min at 4°C. The supernatants were collected for measuring the absorbance at 533 and 650 nm. The relative anthocyanin content was calculated by the following equation: (relative anthocyanin content = (A_{535} − 2 × A_{650})/fresh weight).

RNA isolation and reverse transcription-quantitative polymerase chain reaction analysis

Total RNA was isolated from 8-d-old seedings using the RNA-simple Total RNA Kit (Tiangen, Beijing, China). The complementary DNA (cDNA) was synthesized using the HiScript III RT SuperMix for quantitative polymerase chain reaction (qPCR) (+gDNA wiper) Kit (Vazyme, Nanjing, China) with *c.* 1 μg RNA. Reverse transcription-quantitative polymerase chain reaction reactions were conducted on the CFX96 Real-Time PCR Detection system (Bio-Rad) and QuantStudio 1 (ThermoFisher, Waltham, MA, USA) with a 20 μl total reaction volume containing 10 μl of ChemQ SYBR qPCR Master Mix (Vazyme) and 1 μl cDNA product. The relative expression level of target genes was normalized to the reference gene *ACTIN2* (*AT3G18780*). For each sample, three biological replicates were performed, and each biological replicate contained three technical replicates. Primers used in this study were listed in Supporting Information Table S1.

Immunoblot assay of the phosphorylation status of BRASSINAZOLE RESISTANT 1

Tissue samples collected at different time points were placed in a 2 ml plastic centrifuge tube and ground into fine powder in liquid nitrogen. Protein extraction buffer (50 mM Tris–HCl, pH 7.5, 100 mM NaCl, 10 mM $MgCl_2$, 1 mM EDTA, 10% (v/v) glycerol) was added to resuspend the powder. The protein extracts were centrifuged at 13800 ***g*** for 10 min at 4°C. The supernatants were eluted with 2× SDS gel loading buffer (4% (w/v) sodium dodecyl sulfate (SDS), 0.2% (w/v) bromophenol blue, 20% (v/v) glycerol, 200 mM dithiothreitol (DTT)), separated on a 10% SDS-PAGE gel. The phosphorylation status of BZR1 was detected by anti-GFP monoclonal antibody (Transgene, Beijing, China). The gray value of each band was quantified by the ImageJ tool WBGelDensitometryTool (https://github.com/cernekj/WBGelDensitometryTool).

Microscopy

pBZR1:*BZR1-YFP* transgenic seedlings were first grown on ½MS medium for 1 wk. Seven-day-old seedlings were transferred into ½MS liquid medium for 2 h for preprocessing. The seedlings were then mounted in a –Sul liquid medium (with or without 1 mg ml^{-1} propidium iodide), and the subcellular localization pattern of BZR-YFP was determined using a LSM900 confocal microscope (Zeiss) with an excitation wavelength of 488 nm and an emission wavelength of 509 nm (1% power with a 650 V master gain). For the study of BR-regulated nucleocytoplasmic trafficking of BZR-YFP, seedlings were placed into a –Sul liquid medium containing 1 μM eBL (2,4-Epibrassinolide; Coolaber) or BRZ (Brassinazole; Yuanye, Shanghai, China).

Luciferase transactivation assays

The coding sequence (CDS) sequences of *BZR1* and *BES1* were linked to the *pGreenII 62-SK* (*p62-SK*) vector driven by the *35S* promoter. *p62-SK-BZR1* and *p62-SK-BES1* constructs were used for effector expression, and the empty vector *p62-SK* was used as the negative control. A 2955 bp upstream of the transcription start site of *SULTR1;2* was generated by PCR amplification and was inserted into the *pGreenII-0800-LUC* vector to obtain the luciferase (LUC) reporter vector that expresses *LUC* driven by the *SULTR1;2* promoter: *pGreenII-0800-pSULTR1;2:LUC*. The mixture of effector and reporter was transferred to *Nicotiana benthamiana* for 3 d. LUC luminescence images were collected, and the intensity was quantified by the PlantView100 system (Guangzhou Biolight Biotechnology Co., Ltd). LUC/REN activity was carried out following the protocols for the Dual-Luciferase reporter assay system (Promega). Each sample has five independent transfections. The primers used are listed in Table S1.

AlphaFold3 structure prediction

Protein–DNA complex structures were predicted using the AlphaFold3 online platform (alphafoldserver.com) with auto-generated random seeds. The resulting models were visualized using ChimeraX v.1.8 (Pettersen *et al.*, 2021).

Recombinant protein production and electrophoretic mobility shift assay

The protocol was modified by Unterholzner *et al.* (2017) with slight modifications. The CDS of *BZR1* (*AT1G75080.1*) was cloned in the expression vector pGEX-4T-1 and subsequently transferred into *Escherichia coli* strain BL21(DE3) (Tsingke, Beijing, China). Inoculate 200 ml modified Luria-Bertani (MLB) (10 g l^{-1} peptone, 5 g l^{-1} yeast extract, 5 g l^{-1} NaCl, pH 7.5. Autoclave at 121°C for 20 min) with the overnight culture and incubate at 22°C until the OD_{600} is *c.* 0.5. Add Isopropyl-β-D-thiogalactopyranoside to the culture to a final concentration of 0.2 mM and incubate the culture at 22°C overnight. The recombinant GST-BZR1 fusion protein was purified using Glutathione Sepharose 4B (Cytiva, Uppsala, Sweden) with PBS. After washing with PBS, the fusion proteins were eluted with Elution buffer (150 mM NaCl, 5 mM DTT, 20 mM L-Glutathione reduced, 50 mM Tris–HCl, and pH 8.0).

The *SULTR1;2* promoter fragments containing G-box motif (*CACGTG*) were used for electrophoretic mobility shift assays (EMSA) experiments. Oligos were synthesized by Sangon Biotech Co., Ltd (Shanghai, China) with standard desalting and purified with HPLC. Biotin-labeled 59-mer dsDNAs were mixed with GST-BZR in 10× EMSA binding buffer (250 mM HEPES pH 8.0, 500 mM KCl, 20 mM $MgSO_4$, 10 mM DTT) and 5% (v/v, final concentration) glycerol and incubated for 30 min on ice. The mutated probes (*CACGTG* to *AAAAAA*) were also used. The mixtures were loaded on a 6% polyacrylamide gel, and fluorescence was detected using an Alliance Q9 Advanced system (UVITEC, Cambridge, UK). The sequences of probes used are listed in Table S1.

Chromatin immunoprecipitation assay

ChIP assays were conducted following the protocols established by Nolan *et al.* (2017) with slight modifications. In brief, 1 g of 8-d-old wild-type Col-0 and *pBZR1*:*BZR1-YFP* seedlings were collected and cross-linked for 15 min (release/reapply vacuum once at 7.5 min) in 1% (v/v) formaldehyde solution by vacuum infiltration. Add glycine to a final concentration of 0.125 M to stop cross-linking and apply vacuum for 5 min. Wash the fixed samples with distilled water three times. Dry the samples and freeze them in liquid nitrogen.

The tissue samples were then ground to a fine powder. Add nuclear extraction buffer I (0.4 M sucrose, 10 mM Tris–HCl, pH 8.0, 5 mM β-mercaptoethanol (β-ME), 1 mM PMSF, and protease inhibitor cocktail) to the powder and mix well. The mixture filtered with two layers of Miracloth was centrifuged at 2000 ***g*** for 20 min at 4°C. The pellet was resuspended thoroughly in 1.2 ml nuclear extraction buffer II (0.25 M sucrose, 10 mM Tris–HCl, pH 8.0, 10 mM $MgCl_2$, 1% (v/v) Triton X-100, 5 mM β-ME, 1 mM PMSF, and protease inhibitor cocktail) and centrifuged at 12 000 ***g*** for 10 min at 4°C. The pellet

was resuspended in 400 µl nuclear extraction buffer III (1.7 M sucrose, 10 mM Tris–HCl, pH 8.0, 2 mM $MgCl_2$, 0.15% (v/v) Triton X-100, 5 mM β-ME, 1 mM PMSF, and protease inhibitor cocktail) and centrifuged at 12 000 ***g*** for 60 min at 4°C. The chromatin pellet was then resuspended in 200 µl nuclear lysis buffer (50 mM Tris–HCl, pH 8.0, 10 mM EDTA, 0.5% (w/v) SDS, 5 mM β-ME, 1 mM PMSF, and protease inhibitor cocktail) and diluted with 400 µl ChIP dilution buffer (20 mM Tris–HCl, pH 8.0, 2 mM EDTA, 150 mM NaCl, 1% (v/v) Triton X-100, 5 mM β-ME, 1 mM PMSF, and protease inhibitor cocktail). Mix the chromatin well and the chromatin was sonicated to obtain fragments of *c.* 300 bp using Bioruptor Pico (Diagenode, Lüttich, Belgium) for 6 cycles with 10s on and 50 s off cycle at medium setting. The sonicated chromatin solution was centrifuged at 14 800 ***g*** for 10 min at 4°C. The supernatant was then diluted with ChIP dilution buffer.

The anti-GFP antibody (Transgene) was added and incubated at 4°C overnight. The protein A/G magnetic beads (MCE, Monmouth Junction, NJ, USA) were added to precipitate the chromatin-antibody complexes for 4 h. The beads were washed sequentially with low-salt wash buffer (20 mM Tris–HCl, pH 8.0, 2 mM EDTA, 150 mM NaCl, 1% (v/v) Triton X-100, and 0.1% (w/v) SDS), high-salt wash buffer (20 mM Tris–HCl, pH 8.0, 2 mM EDTA, 500 mM NaCl, 1% (v/v) Triton X-100, and 0.1% (w/v) SDS), LiCl buffer (10 mM Tris–HCl, pH 8.0, 1 mM EDTA, 0.25 M LiCl, 1% (v/v) NP-40, 1% (w/v) sodium deoxycholate), and TE buffer (10 mM Tris–HCl, pH 8.0, 1 mM EDTA). The chromatin complexes were eluted with elution buffer (1% (w/v) SDS, 0.1 M $NaHCO_3$). All the samples were incubated at 65°C overnight. After reverse cross-linking, the proteins were degraded by proteinase K (ThermoFisher) at 45°C for 1 h. The DNA was purified by phenol–chloroform extraction followed by ethanol precipitation. Glycogen (ThermoFisher) was added to facilitate DNA precipitation. Purified DNA was analyzed by ChIP-qPCR. Data were normalized with *ACTIN2* (*AT3G18780*). All primers used in ChIP-qPCR are listed in Table S1.

Measurement of sulfate content

The seedlings were sampled and pretreated as previously mentioned (Fang *et al.*, 2025). After heat digestion, the dry matter was dissolved in ddH_2O and analyzed following the protocol modified by Tabatabai (1974). Briefly, 1 ml of sample was mixed with 100 µl of 0.5 N HCl (prepared by diluting 42 ml of concentrated HCl to 1 l with ddH_2O) in a 2 ml plastic centrifuge tube. Then, 50 µl of barium chloride–gelatin reagent was added to the mixture and mixed thoroughly. The barium chloride–gelatin reagent was prepared as follows: dissolve 0.6 g of gelatin in 200 ml ddH_2O at 65°C, incubate at 4°C overnight, then bring the semi-gelatinous solution to room temperature, add 2.0 g $BaCl_2{\cdot}2H_2O$, and mix until fully dissolved. Store the reagent at 4°C and bring it to room temperature before use.

After 30 min of reaction, the absorbance of the final mixture was determined at 420 nm by spectrophotometer. A standard curve was generated using sulfate solutions at concentrations of 0, 1, 2, 3, 4, and 5 µg ml^{-1}.

Statistical analysis

Data significance was assessed using unpaired *t*-tests (via R function t.test) or ANOVA (using the R package DESCTOOLS v.0.99.59). All statistical figures were generated by the GGPLOT2 package (v.3.4.4). Details on the statistical tests, *P*-values, sample sizes (*n*), and sample types (e.g. root length) are provided in the corresponding figure legends. All experiments were repeated at least three times.

Results

BRASSINAZOLE RESISTANT 1/bri1-EMS-SUPPRESSOR 1 positively regulates S deficiency responses in Arabidopsis

Previous studies demonstrated that BES1 and BZR1 regulate the response to nitrate (N) and phosphorus (P) deficiency in Arabidopsis (Singh *et al.*, 2014; Wang *et al.*, 2023b; Al-Mamun *et al.*, 2024). Notably, recent RNA-seq data also suggested that BR biosynthesis genes are upregulated under S deficiency (Yu *et al.*, 2022). To verify this, we first established an agar-based S-deficient medium, which showed significantly lower sulfate content (Fig. S1a). We then used T-DNA insertion mutants of SULTR1s to verify the S deficiency conditions (Fig. S1b,c). Four-day-old seedlings grown on the ½MS medium (S-sufficient medium, +Sul) were transferred to either S-deficient (−Sul) or S-sufficient (+Sul) medium. The root length of *sultr1;1*, *sultr1;2*, and *sultr1;1*/*sultr1;2* was shorter than wild-type under S deficiency conditions, confirming that the medium was indeed S-deficient.

To investigate the role of BR signaling under S deficiency, we detected the expression of several BR biosynthesis genes (Fig. S2). Increased expression of BR biosynthetic genes is commonly used as an indicator of elevated BR signaling activity (Vukašinović *et al.*, 2021). The results showed that the BR biosynthesis genes were activated under S deficiency conditions within 2 h, supporting the activation of BR signaling under S deficiency conditions. We further assessed the root lengths of BR signaling mutants, including *bri1-301* (a loss-of-function mutant of BR receptor BRI1) and *bin2-3 bil1 bil2* (a loss-of-function mutant of BR kinase BIN2 and its closest homologs). *bri1-301* exhibited shorter root length compared to the wild-type, while *bin2-3 bil1 bil2* showed longer roots (Fig. 1). BR signaling leads to transcriptional responses mediated by its core TFs BZR1/BES1 (Nolan *et al.*, 2020). We next examined the root length in the *bzr1-1D* and *bes1-D* gain-of-function mutants under S deficiency conditions (Fig. 2a,b). Our results showed that the root length of *bzr1-1D* is longer than the wild-type under S deficiency conditions, but there was no significant difference under normal conditions. By contrast, *bes1-D* exhibited no notable phenotype under S deficiency conditions (Fig. 2a,b). The phenotypic response of *bes1-D* under S deficiency did not fully align with our previous observations of BR signaling mutants. To further investigate this discrepancy and to eliminate potential confounding effects from residual S in agar-based media, we employed the long-term hydroponic

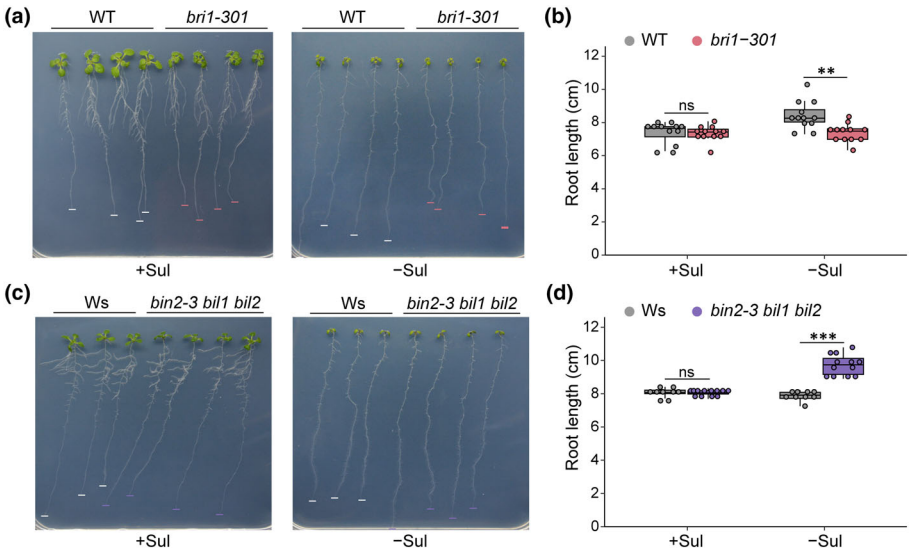

Fig. 1 Brassinosteroid signaling pathway positively regulates Sulphur (S) deficiency response in Arabidopsis seedlings. (a) Phenotypic analysis of wild-type (WT) Col-0 and *bri1-301* mutant under sulfate deficiency conditions. Seeds were germinated on a half-strength Murashige & Skoog (½MS) agar medium for 4 d, then seedlings were transferred to +Sul and −Sul medium for 8 d. (b) Statistical analysis of root length of plants (n = 12) shown in (a). (c) Phenotypic analysis of wild-type Ws and *bin2-3 bil1 bil2* mutant under sulfate deficiency conditions. Seeds were germinated on a ½MS agar medium for 4 d, then seedlings were transferred to +Sul and −Sul medium for 8 d. (d) Statistical analysis of root length of plants (n_{Ws} = 9, $n_{bin2\text{-}3\ bil1\ bil2}$ = 12) shown in (c). Significant differences in (b, d) were determined by two-tailed Student's t-test (**, $P < 0.01$; ***, $P < 0.001$; ns, no significance). Outliers were excluded from the boxplot display for clarity in (b, d). Overlaid dot plots display individual data points with slight jitter to reduce overlap. They are drawn to depict 1.5× the interquartile range as whisker, the 25th and 75th percentiles as upper and lower box limits, and the median as the center line.

culture system to examine the phenotype of *bzr1-1D* and *bes1-D* under S deficiency conditions (Fig. S3). The results showed that both *bzr1-1D* and *bes1-D* have longer root lengths and larger rosettes compared to the wild-type under S deficiency conditions (Fig. S3). S deficiency typically first manifests in plant young leaves with chlorosis and anthocyanin accumulation (de Bang *et al.*, 2021). We next used a sulfate-free liquid culture system to further examine shoot phenotypes (Fig. 2c). Seeds were grown in ½MS liquid medium (+Sul) and −Sul ½MS liquid medium (S-free) for 8 d, respectively. Both *bzr1-1D* and *bes1-D* displayed higher Chl content than the wild-type under S-deficient conditions, suggesting enhanced growth performance (Fig. 2d). The *BES1-RNAi* knockdown line exhibited shorter root length than the wild-type under S deficiency conditions, whereas *bzr1-1D* showed longer roots (Figs 2e,f, S4a,b). Phenotypic analysis of *pBZR1:bzr1-1D-CFP* transgenic plants also showed enhanced tolerance to S deficiency (Fig. S4c,d). Knockout of the *BES1* and *BZR1* showed no significant difference in root length compared to the wild-type under S deficiency (Fig. S4e,f). These results indicate that BR-responsive TFs BZR1 and BES1 positively regulate the response to S deficiency by means independent of canonical BR signaling.

S deficiency promotes the accumulation of BZR1

Since there is phenotypic evidence suggesting that BZR1 and BES1 function redundantly in the response to S deficiency, and that *bzr1-1D* exhibits a better phenotype under S deficiency, we aimed to determine the expression pattern of *BZR1* in Arabidopsis seedlings under S deficiency conditions. We performed qRT-PCR analysis on wild-type seedlings, which were germinated on ½MS agar medium for 8 d, followed by transfer to S-deficient (−Sul) medium (Fig. S5a,b). The *SULTR1;2* expression increased significantly, consistent with previous studies (Fig. S5a) (Aarabi *et al.*, 2016; Yu *et al.*, 2022). However, *BZR1* expression only showed a modest increase of *c.* 1.5-fold after 12 h of treatment (Fig. S5b).

We then employed a 'reverse strategy' to investigate if *BZR1* is an S-deficiency responsive gene. Seeds were pre-treated in sulfate-free liquid medium (S starvation) and then recovered with sulfate for 2 h (S recovery) (Fig. 3a). The expression of *SULTR1;2* was first quantified to verify the effectiveness of this strategy (Fig. S5c). After 2 h of sulfate (1 mM $MgSO_4$) treatment, *BZR1* expression significantly decreased (Fig. 3b). The results indicated that *BZR1* mRNA levels are induced by S deficiency stress and are decreased more than twofold accumulation upon sulfate resupply. By contrast, *BES1* was not found to be an S-deficiency responsive gene (Fig. S5d). To further explore this, we examined the expression of *BZR1*, *BES1*, and their homologs (*BEH*s) in wild-type and *BES1-RNAi* seedlings (Fig. S5e). RT-qPCR result showed that *BZR1* and *BEH3* are S-deficiency responsive genes, with expression levels changing more than twofold. Notably, in *BES1-RNAi*, *BZR1* expression declined more than four-fold within 2 h of sulfate supply, suggesting its rapid responsiveness. To better understand *BZR1* regulation in the BR pathway, we also detected *BZR1* expression in additional BR signaling mutants, including *bri1-301* and *bin2-3 bil1 bil2*, with *SULTR1;2* expression serving as a reference (Fig. S5f). In wild-

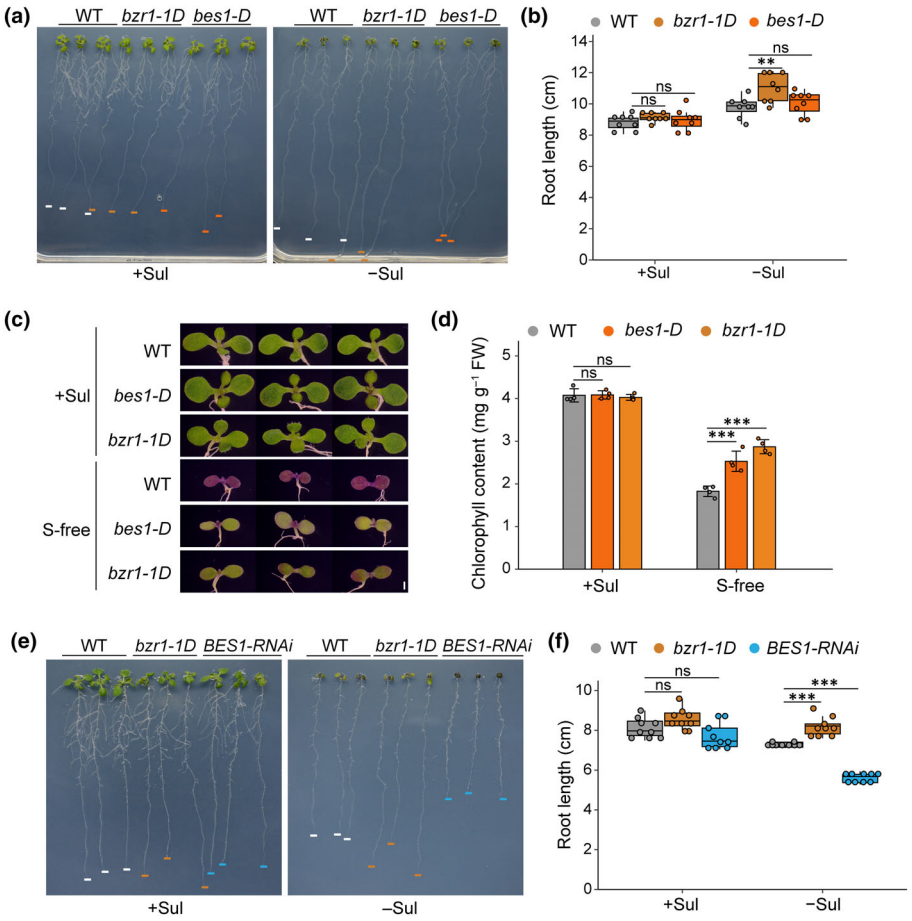

Fig. 2 BRASSINAZOLE RESISTANT 1 (BZR1)/bri1-EMS-SUPPRESSOR 1 (BES1) mediate brassinosteroid signaling-regulated response to S deficiency. (a) Phenotypic analysis of Arabidopsis wild-type (WT) Col-0, *bes1-D*, and *bzr1-D* mutants under S deficiency conditions. Seeds were germinated on half-strength Murashige & Skoog (½MS) agar medium (+Sul) for 4 d, then seedlings were transferred to +Sul and −Sul medium for 8 d. (b) Statistical analysis of root length of plants (n = 8) shown in (a). (c) Phenotypic analysis of Arabidopsis wild-type Col-0, *bes1-D*, and *bzr1-D* under hydroponic S-free conditions. Seeds were germinated in ½MS liquid medium (+Sul) and −Sul ½MS liquid medium (S-free) for 8 d, respectively (Bar, 1 mm). (d) Statistics analysis of Chl content of plants (n = 4) shown in (c). Data are means ± SD of plants. (e) Phenotypic analysis of Arabidopsis wild-type Col-0, *bzr1-1D*, and *BES1-RNAi* under sulfate deficiency conditions. Seeds were germinated on ½MS agar medium for 4 d, then seedlings were transferred to +Sul and −Sul medium for 8 d. (f) Statistical analysis of root length of plants (n = 9) shown in (e). Significant differences were determined by Dunnett's test for multiple comparisons (**, $P < 0.01$; ***, $P < 0.001$; ns, no significance). Outliers were excluded from the boxplot display for clarity in (b, f). Overlaid dot plots display individual data points with slight jitter to reduce overlap. They are drawn to depict 1.5× the interquartile range as whisker, the 25th and 75th percentiles as upper and lower box limits, and the median as the center line.

type (Col-0 and Ws) and *bri1-301*, the expression trends of *BZR1* and *SULTR1;2* were similar before and after sulfate resupply. However, in *bin2-3 bil1 bil2*, the expression of *BZR1* exhibited an opposite trend compared to *SULTR1;2*, suggesting that the loss of BIN2 and its homologs strongly influences *BZR1* accumulation, contributing to the more than two-fold increase observed under S deficiency. Together, these results highlighted the role of BIN2-mediated dephosphorylation and activation of BZR1 in the S deficiency response.

To investigate the protein dynamics of BZR1 under S deficiency, we carried out a time-course analysis of seedlings collected at different time points. We measured the abundance of BZR1 (the unphosphorylated, activated form) and its phosphorylated, inactivated form (BZR1p). BZR1 accumulated *c.* 2.5 times more than the basal level by 48 h under S deficiency conditions (Fig. 3c). Furthermore, we examined the relationship among BZR1 synthesis, accumulation, and degradation under S deficiency by applying cycloheximide (CHX) and MG132. BZR1 protein levels were detected by immune blotting at 6, 12, 24, and 48 h (Fig. 3d). CHX inhibits protein synthesis, while MG132 blocks proteasomal degradation. Compared with mock treatment (dimethyl sulfide, DMSO), the accumulation of BZR1, especially BZR1p, was more pronounced under S deficiency with MG132 treatment. By contrast, the BZR1 protein level decreased rapidly when treated with CHX. Treatment with both CHX and MG132 showed slower degradation than with CHX alone. Our results indicated that BZR1 synthesis is induced by S deficiency, and the 26S proteasome-dependent degradation of BZR1 occurs concurrently.

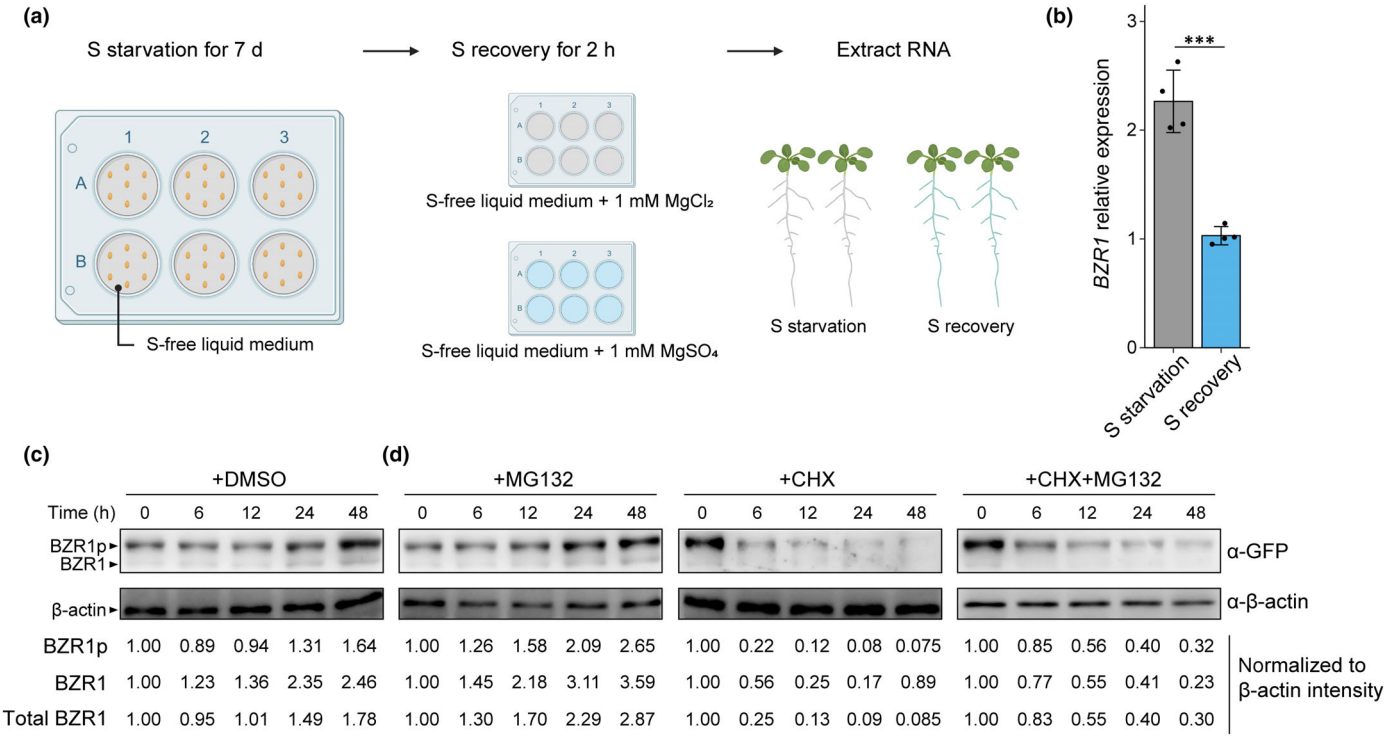

Fig. 3 Sulphur deficiency activates the expression and dephosphorylation of BRASSINAZOLE RESISTANT 1 (BZR1). (a) Schematic diagram illustrating the identification of S-deficiency responsive genes in Arabidopsis. Seeds were germinated in S-free liquid medium for 7 d, then seedlings were treated with fresh S-free liquid medium containing 1 mM $MgCl_2$ (S starvation) or $MgSO_4$ (S recovery). Figure was created via BioRender (BioRender.com/9cr0bnh). (b) *BZR1* is an S-deficiency responsive gene in Arabidopsis. Seeds germinated in S-free liquid medium for 7 d were treated with sulfate (1 mM $MgSO_4$) or $MgCl_2$ (control) for 2 h. Reverse transcription-quantitative polymerase chain reaction (RT-qPCR) analyses were performed. Mean ± SD ($n = 4$). Significant differences were determined by two-tailed Student's *t*-test (***, $P < 0.001$). (c) Immunoblot analysis of BZR1 protein in Arabidopsis *pBZR1:BZR1-YFP* seedlings under S deficiency conditions. Seedlings were treated with DMSO (Mock), (d) 50 μM MG132 (+MG132), 100 μM CHX (+CHX), 100 μM CHX + 50 μM MG132 (+CHX + MG132) under S deficiency conditions. Samples were collected at indicated time points. The intensity of BZR1 and BZR1p was normalized according to the intensity of β-actin. The sample loads were the same at 0 h across all four treatments and were set as 1. CHX, cycloheximide; DMSO, dimethyl sulfide.

S deficiency induces the relocation of cytoplasmic BZR1 to the nucleus

A previous study elegantly demonstrated that BZR1 was recruited from the cytosol to the nucleus within 30 min after supplying 1 μM eBL (Wang *et al.*, 2021). We have already proved that BZR1 responds to S deficiency via BR signaling according to the genetic and molecular approaches. To explore whether an S-deficient environment could recruit the cytoplasmic BZR1 to the nucleus, we conducted confocal fluorescing using transgenic plant expression BZR1-YFP fusion protein driven by the native *BZR1* promoter (*pBZR1:BZR1-YFP*) under S deficiency (−Sul) condition. We treated the seedlings with four conditions: +Sul, −Sul, −Sul + eBL, and −Sul + BRZ. Both −Sul and −Sul + eBL could induce the relocation of cytoplasmic BZR1 into the nucleus. Supplying BRZ could inhibit the relocation of cytoplasmic BZR1 induced by S deficiency. The results showed that S deficiency could induce the relocation of BZR1 within 30 min of S deficiency treatment (Fig. 4a,b). To avoid the effect of multi-exposure to the fluorescence, we shot confocal fluoresce imaging again at 30 min (Fig. 4c). This experiment demonstrated that cytoplasmic BZR1 can be recruited to the nucleus under S deficiency, and the process is BR dependent.

BRASSINAZOLE RESISTANT 1 directly targets the *SULTR1;2* promoter *in vitro* and *in vivo*

The response of BZR1 under S deficiency is noted above, but its regulatory targets remain to be identified. The binding motifs of BZR1 are well demonstrated for G-box (*CACGTG*) and BR-response element (BRRE; $CGTG^{C}/_{T}G$) in promoter regions (Oh *et al.*, 2012). We focused on the primary S uptake in plants from soil, specifically investigating whether the transporters *SULTR1;1* and *SULTR1;2*, which are involved in this process, are regulated by BZR1. Both transporters show significantly increased expression under S deficiency (Aarabi *et al.*, 2016; Yu *et al.*, 2022). Previous research on core promoter prediction in plants gave us a hint for determining the boundaries of the promoters for *SULTR1;1* and *SULTR1;2* (Jores *et al.*, 2021). Based on these data, we analyzed the promoter sequences of the two transporters. We found two G-box motifs in the promoter of *SULTR1;2*,

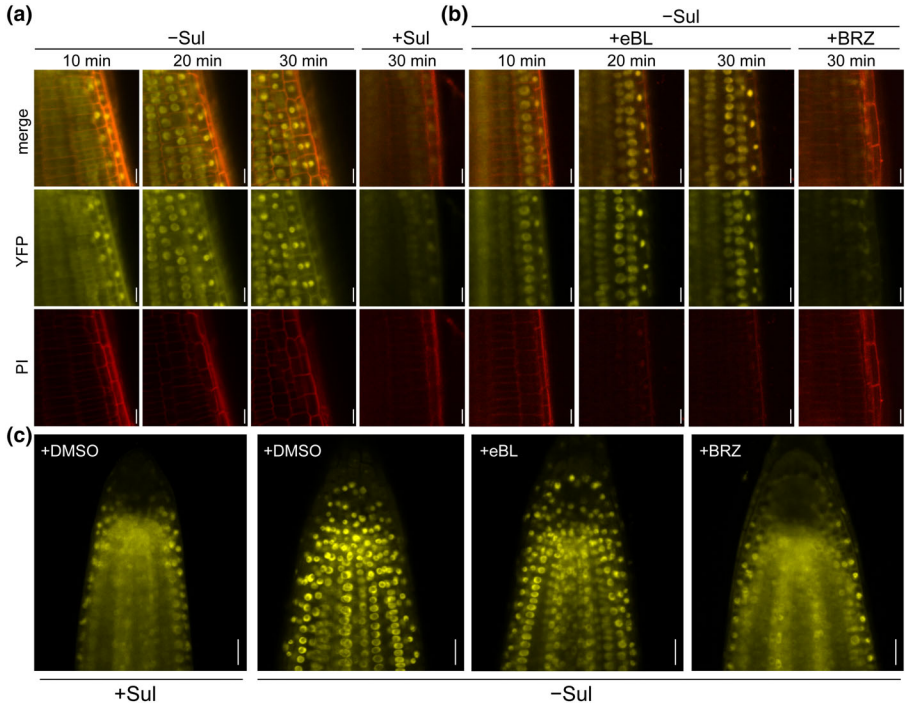

Fig. 4 The relocation of cytoplasmic BRASSINAZOLE RESISTANT 1 (BZR1) to the nucleus is promoted by sulfur deficiency and brassinosteroid. Transgenic Arabidopsis seedlings harboring *pBZR1:BZR1-YFP* were grown on half-strength Murashige & Skoog (½MS) medium for 7 d under long-day (LD) conditions. The fluorescence signal of BZR1-YFP was then examined. The seedlings were treated with (a) ½MS liquid medium without sulfate and (b) ½MS liquid medium without sulfate +1 mM eBL. YFP fluorescence was observed every 10 min. Control treatments included ½MS liquid medium and ½MS liquid medium without sulfate + 1 mM BRZ. BRZ, Brassinazole; eBL, 24-Epibrassinolide; PI, propidium iodide. (c) Confocal microscopy was used to examine the subcellular localization of BZR1-YFP. Transgenic Arabidopsis seedlings harboring *pBZR1:BZR1-YFP* were grown on ½MS medium for 7 d. The fluorescence signal of BZR1-YFP was examined. Seedlings were treated with ½MS liquid medium (control), ½MS liquid medium without sulfate, ½MS liquid medium without sulfate + 1 mM eBL, and ½MS liquid medium without sulfate + 1 mM BRZ for 30 min. YFP fluorescence was observed (Bars, 10 μm). DMSO, dimethyl sulfide; YFP, yellow fluorescent protein.

while no potential regulatory elements (either G box or BRRE element) were observed in the promoter of *SULTR1;1*. Therefore, we hypothesize that BZR1 might directly regulate the expression of sulfate transporter *SULTR1;2* to respond to the S deficiency.

Previous ChIP–chip data showed that BZR1 binds to two sites on the *SULTR1;2* promoter (Sun *et al.*, 2010). Additionally, ChIP-seq data from two studies identified binding peaks on the *SULTR1;2* promoter (Oh *et al.*, 2014; Zhu *et al.*, 2024). To investigate the *in vivo* binding of BZR1 to the *SULTR1;2* promoter, we conducted LUC-activated assays and dual-luciferase reporter assays. The results indicated that BZR1 could enhance the expression of *SULTR1;2* (Fig. 5a,d). We also conducted a dual-luciferase reporter assay with BES1, which similarly upregulated *SULTR1;2* expression, although with a lower LUC/REN ratio compared to BZR1 (Fig. S6). Having identified that BZR1 promoted the expression of *SULTR1;2*, we sought to determine whether BZR1 could directly interact with the promoter of *SULTR1;2*. The crystal structure of the BZR1 DNA binding domain has been previously resolved, providing a basis for structural modeling (Nosaki *et al.*, 2018). We used AlphaFold3 to predict potential protein–DNA interactions. Promoter analysis using PLANTPAN 4.0 identified three putative BZR1 binding sites on the *SULTR1;2* promoter: two canonical G-box motifs (*CACGTG*) and one G-box-like motif (*CACGTAG*) located downstream of the core promoter (Chow *et al.*, 2024). To evaluate the predicted binding, we generated structural models of BZR1 in complex with 59-nt DNA fragments containing either normal or mutated motifs (Fig. S7). Furthermore, when binding motifs were mutated, the predicted binding domain of BZR1 shifted away from the DNA interface, supporting the importance of the binding motifs (Fig. S7). The interface predicted TM score (ipTM) and predicted alignment TM score (pTM) were used to estimate the confidence of the protein–DNA interaction (Abramson *et al.*, 2024). Models with canonical G-box motifs showed notably higher ipTM and pTM scores, while the difference between wild-type and mutant in the G-box-like group was minimal, suggesting a lack of specific binding to the noncanonical motif in regulating *SULTR1;2* expression (Fig. 5e). Thus, to confirm whether BZR1 directly binds to the G-box motifs of *SULTR1;2*, we conducted EMSA using purified BZR1 protein fused with GST tag. The results indicated that BZR1 physically binds to the 59-nt *SULTR1;2* promoter fragments *in vitro*, and this binding was competed by wild-type probes but not by mutated probes, which were consistent with the prediction results (Figs 5f, S7). *In vivo* binding of BZR1 to the *SULTR1;2*

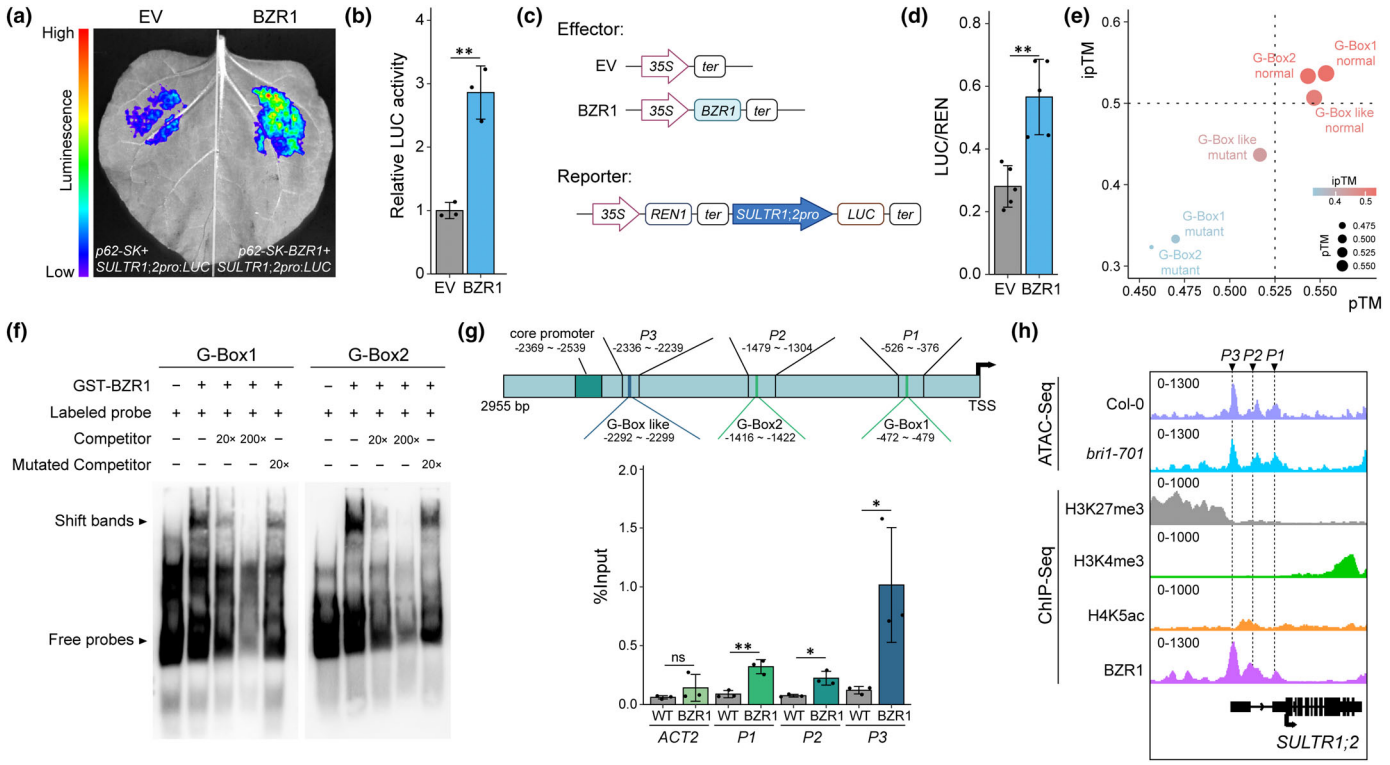

Fig. 5 BRASSINAZOLE RESISTANT 1 (BZR1) directly binds to the *SULTR1;2* promoter *in vitro* and *in vivo*. (a, b) LUC activation assay showing that AtBZR1 activates the At*SULTR1;2* promoter in *Nicotiana benthamiana* leaves. (b) Data analysis of relative LUC activity in (a). The intensity of BZR1 was normalized to the empty vector (EV) within the same leaf ($n = 3$). (c, d) Dual-LUC assay indicating that AtBZR1 activates the At*SULTR1;2* promoter in *N. benthamiana* leaves. (d) Data analysis of relative LUC/REN ratio from dual-LUC assay in (c). The ratio of LUC to REN represents the activity of the *SULTR1;2* promoter in the absence or presence of BZR1 ($n = 5$). LUC, firefly luciferase; REN, renilla luciferase; ter, terminator sequence. (e) AlphaFold3 predicted ipTM and pTM scores. Dimers of BZR1 DNA binding domain bound to 59-nt DNA fragments containing G-Box or G-Box-like motifs were plotted. Scores from three independent predictions were averaged and plotted. (f) Electrophoretic Mobility Shift Assay (EMSA) showing the binding of AtBZR1 to the G-box motif of the At*SULTR1;2* promoter *in vitro*. The shift bands indicated BZR1 binding to the two G-box motifs of the *SULTR1;2* promoter with biotin labels. Competitive assays were performed using 20× and 200× unlabeled wild-type probes (Competitor). Mutated competitor, mutant G-box (CAGATG to AAAAAA). (g) ChIP assay showing BZR1 occupancy at the three sites on *SULTR1;2* promoter in Arabidopsis. The *ACTIN2* was used as a reference. Mean ± SD from three biological replicates. Significant differences in (b, d, g) were determined by two-tailed Student's *t*-test (*, $P < 0.05$; **, $P < 0.01$; ns, no significance). (h) Integrative Genomics Viewer (IGV) visualization of published omics-data at *SULTR1;2*. ATAC-seq reads show the chromatin accessibility around *SULTR1;2* in Arabidopsis wild-type Col-0 and *bri1-701* mutant (Zhu *et al*., 2024). ChIP-seq data of three histone modification markers (H3K4me3 and H4K5ac for activation and H3K27me3 for repression) and BZR1 illustrate the distribution of histone modification markers and BZR1 around *SULTR1;2* (Zhu *et al*., 2024). The black diagrams underneath the tracks indicate gene structure of *SULTR1;2*. ChIP, chromatin immunoprecipitation; ChIP-Seq, ChIP sequencing; ipTM, interface predicted TM score; pTM, predicted alignment TM score.

promoter was further confirmed by ChIP-qPCR analysis using Col-0 and *pBZR1:BZR1-YFP* plants (Fig. 5g). *P1* (containing G-Box1) and *P2* (containing G-Box1) each contained a G-box motif, while *P3* contained a G-box-like motif. Interestingly, three prominent binding tracks observed in previous ChIP-seq data were consistent with our ChIP-qPCR assay results (Fig. 5h). Additionally, the transcription activation mark H4K5ac was enriched at *P1* and *P2* regions but not at *P3* (Fig. 5h). These epigenetic data suggest that the binding peak of BZR1 at *P3* may not contribute to the direct transcriptional regulation of *SULTR1;2*, which is consistent with the AlphaFold3 prediction scores at this site (Figs 5e,g, S7). However, the functional relevance of the P3 binding site remains to be determined in future studies. Our results strongly suggested that BZR1 directly binds to the *SULTR1;2* promoter via two canonical G-box motifs and one noncanonical motif that closely resembles a G box.

BRASSINAZOLE RESISTANT 1 promotes sulfate uptake by targeting *SULTR1;2*

To confirm the results above genetically, we crossed *bzr1-1D* with *sultr1;2* to generate the *bzr1-1D*/*sultr1;2* line. When *SULTR1;2* expression was knocked down in *bzr1-1D*, the root length of *bzr1-1D*/*sultr1;2* was shorter than that of *bzr1-1D* under S deficiency conditions (Figs 6a,b, S8). In addition, to investigate whether the activation of *SULTR1;2* by BZR1 was BR dependent, we applied the BR synthesis inhibitor BRZ under S deficiency conditions. The results showed that BRZ treatment abolished the tolerance phenotype of wild-type Col-0 under S deficiency, making it comparable to the *sultr1;2* mutant (Fig. S9).

A previous study reported that sulfate promotes true leaf development (Yu *et al*., 2022). We conducted the shoot apex growth

New Phytologist

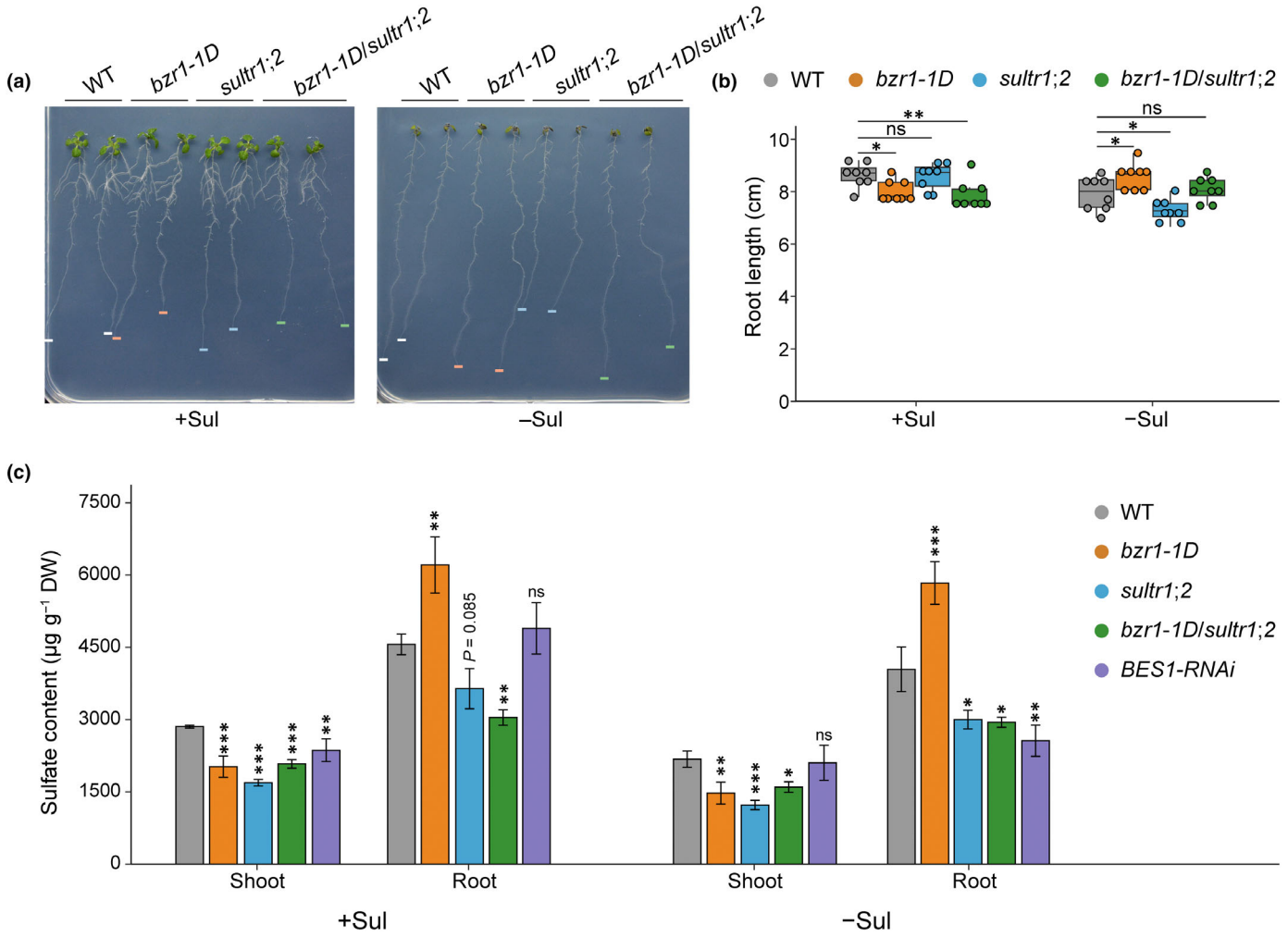

Fig. 6 BRASSINAZOLE RESISTANT 1 (BZR1) positively regulates sulfate accumulation by requiring *SULTR1;2*. (a) Phenotypic analysis of Arabidopsis wild-type (WT) Col-0, *bzr1-1D*, *sultr1;2*, and *bzr1-1D/sultr1;2* mutants under sulfate deficiency conditions. (b) Statistics analysis of root length of plants (n = 8) shown in (a). Outliers were excluded from the boxplot display for clarity. Overlaid dot plots display individual data points with slight jitter to reduce overlap. They are drawn to depict 1.5× the interquartile range as whiskers, the 25th and 75th percentiles as upper and lower box limits, and the median as the center line. (c) Sulfate content in Arabidopsis wild-type Col-0, *bzr1-1D*, *sultr1;2*, *bzr1-1D/sultr1;2*, and *BES1-RNAi* under 7 d of S deficiency treatment. Data are means ± SD of sulfate S content of plants (n = 3). Significant differences in (b, c) were determined by Dunnett's test for multiple comparisons (*, $P < 0.05$; **, $P < 0.01$; ***, $P < 0.001$; ns, no significance). DW, dry weight.

analysis, in which the results showed a similar phenotype to the root length results (Fig. S10). Interestingly, we also observed a darker coloration in the shoots after S deficiency treatment. A recent study reported that BZR1 interacts with PAP1/PAP2 to positively regulate anthocyanin production, and that nitrogen deficiency activates the BZR1–PAP1/PAP2 module (Lee *et al.*, 2024). To investigate whether a similar mechanism is involved under S deficiency, we measured anthocyanin content in *bzr1-1D* seedlings. The results showed increased anthocyanin accumulation in *bzr1-1D*. (Fig. S11). It is convincing that both S and nitrogen deficiencies may promote anthocyanin biosynthesis through a common BZR1–PAP1/PAP2 regulatory pathway.

We further analyzed the sulfate content and found that *bzr1-1D* had higher sulfate content than wild-type, while *bzr1-1D/sultr1;2* had lower sulfate content than wild-type (Fig. 6c). These results confirmed that BZR1 promotes sulfate uptake primarily by regulating *SULTR1;2*. To examine the involvement of additional key BR signaling components, we also determined sulfate content in *bri1-301* and *bin2-3 bil1 bil2* mutants (Fig. S12). Consistent with their root length phenotypes, *bri1-301* showed lower sulfate content, whereas *bin2-3 bil1 bil2* showed higher sulfate content (Figs 1, S12).

Taken together, these findings demonstrate that *SULTR1;2* is a downstream target of BZR1 in Arabidopsis, and that BZR1-mediated BR signaling controls sulfate uptake by regulating *SULTR1;2* expression under S deficiency.

Discussion

In this study, we identified a direct molecular connection between BZR1 and the sulfate transporter SULTR1;2 which facilities sulfate uptake from the environment (Fig. 7). We propose that BR

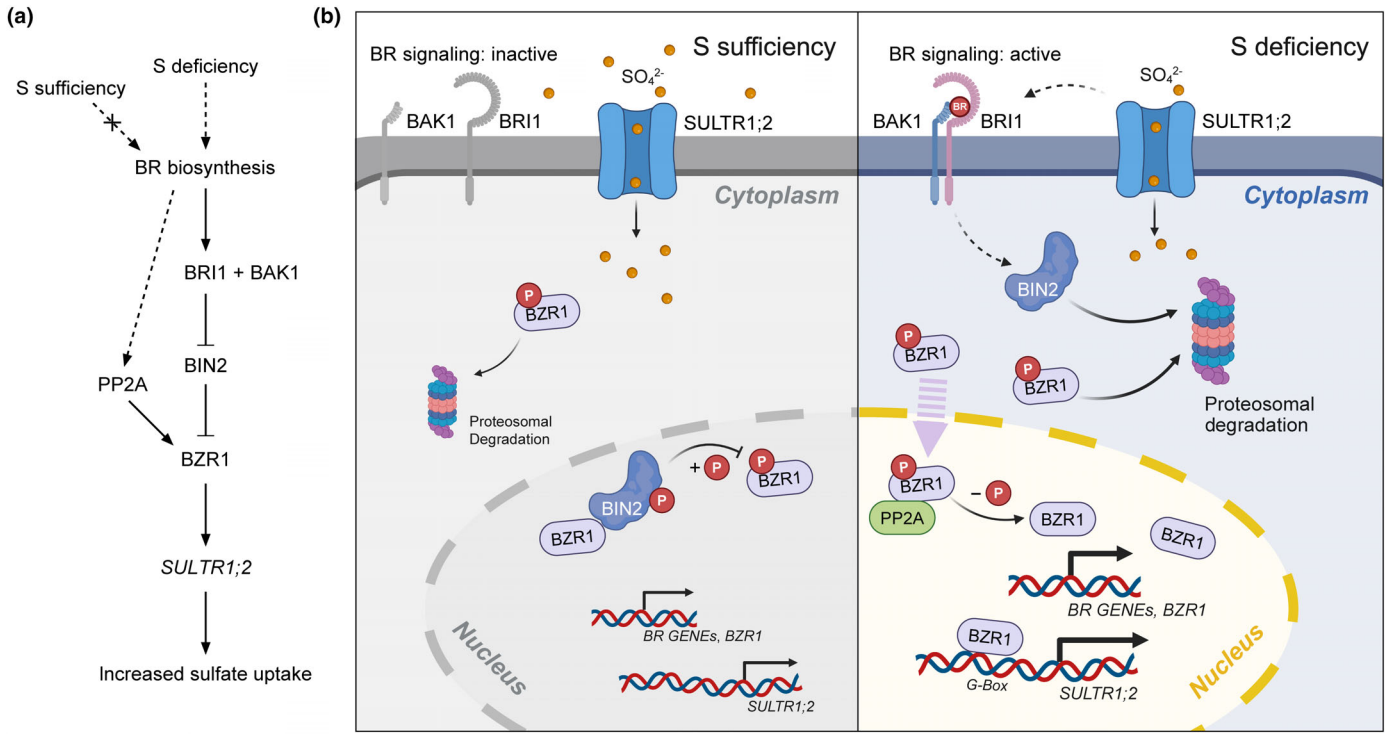

Fig. 7 Working model for BRASSINAZOLE RESISTANT 1 (BZR1)-mediated brassinosteroid (BR) signaling in response to sulfur (S) deficiency. (a) A schematic diagram illustrating BZR1 mediated BR signaling in response to S deficiency in Arabidopsis. S deficiency activates the BR biosynthesis. Newly synthesized BR binds to the BR receptor BRI1, together with BAK1, leading to dephosphorylation, deactivation, and degradation of BIN2 kinase. BIN2 inactivation indirectly promotes the dephosphorylated BZR1 accumulation, which is mediated by protein phosphatase 2A (PP2A). Activated BZR1 then induces *SULTR1;2* expression, enhancing sulfate uptake. (b) A proposed model of the regulation of BR signaling in response to S deficiency in Arabidopsis. Under S sufficiency (left), BZR1 is phosphorylated by active BIN2 and targeted for degradation by the 26S proteasome. Upon S deficiency (right), BR biosynthesis genes are upregulated, activating BR signaling. This triggers BIN2 dephosphorylation and degradation. Cytoplasmic BZR1 translocates to the nucleus, where PP2A-mediated dephosphorylation activates it. Activated BZR1 binds G-Box motifs in the promoter of *SULTR1;2*, inducing expression and increasing sulfate uptake. Thicker arrows indicate enhanced processes under S deficiency: BR biosynthesis, BZR1 synthesis and degradation, and *SULTR1;2* expression. Solid arrows indicate positive direct regulation, dashed arrows indicate indirect regulation, and blunt arrows represent negative regulation. Figure (b) was created via BioRender (BioRender.com/y81a808). BAK1, BRI1-ASSOCIATED RECEPTOR KINASE 1; BRI1, BRASSINOSTEROID INSENSITIVE 1.

signaling regulates sulfate uptake in response to S deficiency, supported by the upregulation of several BR biosynthesis genes in published transcriptome data under S-deficient conditions. Previous studies have shown that nitrogen (N) and phosphorus (P) deficiencies activate BR signaling and transcription regulation mediated by BZR1/BES1 TF family (Singh *et al.*, 2014; Wang *et al.*, 2023b; Al-Mamun *et al.*, 2024). To explore this further, we introduced the concept of 'S deficiency responsive gene' to identify genes which significantly change under long-term nutrient deficiency and recovered within hours (Fig. 3a). This helped us to elucidate the role of BZR1 under S deficiency.

The key finding from the model is that both the synthesis and degradation of BZR1 occur in the cell under S deficiency conditions (Fig. 3c,d). This mechanism likely maintains high transcriptional efficiency of target genes by supplying newly synthesized BZR1 (Spoel *et al.*, 2009). Recent studies have shown that BR-induced BZR1 translocation into the nucleus happens within 30 min, mediated by BIN2/PP2A (Wang *et al.*, 2021). Moreover, BR treatment activates both the synthesis and degradation of BZR1 (Wang *et al.*, 2021), further supporting our findings that S deficiency activates BR signaling. Using AlphaFold3 structure predictions, we developed models visualizing potential binding interactions (Figs 5d, S7). Integration of omics data also allowed us to observe the chromatin state of the *SULTR1;2* promoter (Fig. 5h). Combining these predictions with BZR1 ChIP data, H4K5ac ChIP data (a transcription activation mark), and *in vitro* and *in vivo* binding assays, we determined that the G-box-like motif bound by BZR1 likely does not confer transcriptional activation (Figs 5e–h, S7). This finding aligns with recent research indicating that TF DNA binding is not invariably linked to transcription regulation (Mahendrawada *et al.*, 2025). These advanced approaches provide an exciting opportunity to further dissect the molecular mechanisms underlying BZR1-mediated BR-responsive transcriptional regulation of *SULTR1;2* under S deficiency.

Regarding the degradation of BZR1 through the 26S proteasome under S deficiency, the mediators of this process remain unknown. Recent studies have suggested that the plant U-box protein PUB40 mediates BZR1 degradation in a root-specific manner, while COP1, a RING E3 ubiquitin ligase downstream of photoreceptors, regulates BZR1 stability under different light conditions (Kataoka *et al.*, 2004b; Kim *et al.*, 2019). Another study reported

that in the loss-of-function mutant of RPT2a, a 26S proteasome subunit, the expression patterns of S assimilation and ubiquitin degradation pathways are altered (Wawrzyńska & Sirko, 2020). However, the exact regulators involved in BZR1 degradation under S deficiency remain to be identified in future research.

Our data show that the recruitment of cytoplasmic BZR1 under S deficiency starts within 20 min, which is a rapid response (Fig. 4). The transport of cytoplasmic BZR1 into the nucleus requires nuclear importins. A recent study performed a yeast two-hybrid assay that identified interactions between BZR1 and importins, including KA120, which plays a key role in plant immunity regulation (Wang *et al.*, 2021; Jia *et al.*, 2023). We are interested in whether this importin also responds to S deficiency, which could link plant growth and defense (Zhang *et al.*, 2023). Furthermore, a recent study demonstrated that BZR1 activates S metabolism, suggesting that BZR1 may be another master regulator in the S deficiency response like SLIM1 (M. Wang *et al.*, 2023). Supporting this, *SULTR1;2* expression shows distinct patterns in BES1-RNAi, *bri1-301*, and *bin2-3 bil1 bil2* mutants under S starvation and recovery conditions (Fig. S5e,f). This observation suggests that BR signaling is not the sole pathway responding to S deficiency, potentially implicating alternative mechanisms such as SLIM1-mediated S signaling. The potential interaction between SLIM1 and BZR1 in response to S deficiency remains for future investigation.

Another question arises from our observation that the gain-of-function mutant *bzr1-1D* shows a phenotype of root length under S deficiency, whereas *bes1-D* does not (Fig. 2a,b). However, *bes1-D* displays significant shoot and root phenotypes in hydroponics (Fig. 2c–g). Though we found that *BES1* expression does not increase under S deficiency, a dual-luciferase assay showed that BES1 can activate *SULTR1;2* expression, albeit with a lower LUC/REN ratio compared to BZR1 (Figs S4d, S6). Based on the results, we noted that BZR1 is the major TF to conduct BR signaling in response to S deficiency, though BES1 and BZR1 function redundantly in BR signaling (Figs 2, S4c,d, S6).

S, as a key macronutrient, is often overlooked in plant nutrition research (Ristova & Kopriva, 2022; Wang *et al.*, 2023a). The risk of S deficiency in agriculture is increasing due to reduced emission of SO_2 (Wang *et al.*, 2018; Aas *et al.*, 2019; Hinckley *et al.*, 2020). Therefore, when considering strategies to manifest BR signaling for crop improvement (e.g. enhancing stress tolerance or yield), optimizing S nutrition and understanding its impact on the BZR1-*SULTR1;2* module is crucial. The posttranslational regulatory mechanisms of the sulfate transporters, such as phosphorylation, remain poorly understood (Wang *et al.*, 2023a). Liquid–liquid phase separation (LLPS) has been shown to regulate a broad range of abiotic stress responses; however, its role in S deficiency remains unexplored (Liu *et al.*, 2023). It is crucial to address the 'missing link' S in plant nutrition in future studies.

Acknowledgements

All work was performed in collaboration. We thank Zhiyong Wang (Stanford University, USA), Peng Wang (Nanjing Agriculture University, China), Jia Li (Guangzhou University, China), Dawei Zhang (Sichuan University, China), Hongtao Liu (Shenzhen University, China), and Wenfei Wang (Fujian Agriculture and Forestry University, China) for material assistance. In addition, we thank Dr Qiong Zhang, Dr Hua Zhao, Dr Xueling Huang, Dr Fengping Yuan, and Technician Xiaona Zhou (State Key Laboratory for Crop Stress Resistance and High-Efficiency Production) for providing ZEISS LSM900, CFX connect, QuantStudio 1, and other platforms. This work was supported by the National Natural Science Foundation of China (32222008 to CW) and China Postdoctoral Science Foundation (2024M762635 to TW) and by The Interdisciplinary Frontier Innovation Team Program of Northwest A&F University (A1080524001) and the Chinese Universities Scientific Fund (2452023069).

Competing interests

None declared.

Author contributions

CW, TW, and XC conceived the original idea and designed the experiments. XC, ZY, WG, and YZ performed the experiments. XC analyzed data and wrote the manuscript with contributions from all authors. CW and TW directed the project and revised the manuscript.

ORCID

Xuanyi Chen https://orcid.org/0000-0002-8822-5903
Wendi Guo https://orcid.org/0009-0000-5869-6088
Cun Wang https://orcid.org/0000-0002-9470-1945
Tian Wang https://orcid.org/0009-0006-7472-0256
Zhenghao Yu https://orcid.org/0009-0005-4344-7608
Yuting Zhou https://orcid.org/0009-0008-4736-8079

Data availability

All the data and materials that support the findings of this study have been included as part of the article or as Fig. S7 (Pettersen *et al.*, 2021; Abramson *et al.*, 2024). The ChIP-seq and ATAC-seq data were downloaded from GEO: GSE233416.

References

Aarabi F, Kusajima M, Tohge T, Konishi T, Gigolashvili T, Takamune M, Sasazaki Y, Watanabe M, Nakashita H, Fernie AR *et al.* 2016. Sulfur deficiency–induced repressor proteins optimize glucosinolate biosynthesis in plants. *Science Advances* **2**: e1601087.

Aas W, Mortier A, Bowersox V, Cherian R, Faluvegi G, Fagerli H, Hand J, Klimont Z, Galy-Lacaux C, Lehmann CMB *et al.* 2019. Global and regional trends of atmospheric sulfur. *Scientific Reports* **9**: 953.

Abramson J, Adler J, Dunger J, Evans R, Green T, Pritzel A, Ronneberger O, Willmore L, Ballard AJ, Bambrick J *et al.* 2024. Accurate structure prediction of biomolecular interactions with AlphaFold 3. *Nature* **630**: 493–500.

Al-Mamun MH, Cazzonelli CI, Krishna P. 2024. BZR1 and BES1 transcription factors mediate brassinosteroid control over root system

architecture in response to nitrogen availability. *Frontiers in Plant Science* **15**: 1387321.

de Bang TC, Husted S, Laursen KH, Persson DP, Schjoerring JK. 2021. The molecular–physiological functions of mineral macronutrients and their consequences for deficiency symptoms in plants. *New Phytologist* **229**: 2446–2469.

Barberon M, Berthomieu P, Clairotte M, Shibagaki N, Davidian J-C, Gosti F. 2008. Unequal functional redundancy between the two Arabidopsis thaliana high-affinity sulphate transporters SULTR1;1 and SULTR1;2. *New Phytologist* **180**: 608–619.

Chaiwanon J, Wang Z-Y. 2015. Spatiotemporal Brassinosteroid signaling and antagonism with auxin pattern stem cell dynamics in Arabidopsis roots. *Current Biology* **25**: 1031–1042.

Chen W, Lv M, Wang Y, Wang P-A, Cui Y, Li M, Wang R, Gou X, Li J. 2019. BES1 is activated by EMS1-TPD1-SERK1/2-mediated signaling to control tapetum development in *Arabidopsis thaliana*. *Nature Communications* **10**: 4164.

Chen Z, Zhao P-X, Miao Z-Q, Qi G-F, Wang Z, Yuan Y, Ahmad N, Cao M-J, Hell R, Wirtz M *et al.* 2019. SULTR3s function in chloroplast sulfate uptake and affect ABA biosynthesis and the stress response. *Plant Physiology* **180**: 593–604.

Chow C-N, Yang C-W, Wu N-Y, Wang H-T, Tseng K-C, Chiu Y-H, Lee T-Y, Chang W-C. 2024. PlantPAN 4.0: updated database for identifying conserved non-coding sequences and exploring dynamic transcriptional regulation in plant promoters. *Nucleic Acids Research* **52**: D1569–D1578.

Fang Y, Ju C, Javed L, Cao C, Deng Y, Gao Y, Chen X, Sun L, Zhao Y, Wang C. 2025. Plasma membrane-associated calcium signaling modulates zinc homeostasis in Arabidopsis. *Science Bulletin* **70**: 1478–1490.

Fernández JD, Miño I, Canales J, Vidal EA. 2024. Gene regulatory networks underlying sulfate deficiency responses in plants. *Journal of Experimental Botany* **75**: 2781–2798.

Gao H, Wang C, Li L, Fu D, Zhang Y, Yang P, Zhang T, Wang C. 2020. A novel role of the calcium sensor CBL1 in response to phosphate deficiency in *Arabidopsis thaliana*. *Journal of Plant Physiology* **253**: 153266.

González-García M-P, Vilarrasa-Blasi J, Zhiponova M, Divol F, Mora-García S, Russinova E, Caño-Delgado AI. 2011. Brassinosteroids control meristem size by promoting cell cycle progression in Arabidopsis roots. *Development* **138**: 849–859.

Han C, Wang L, Lyu J, Shi W, Yao L, Fan M, Bai M-Y. 2023. Brassinosteroid signaling and molecular crosstalk with nutrients in plants. *Journal of Genetics and Genomics* **50**: 541–553.

He J-X, Gendron JM, Sun Y, Gampala SSL, Gendron N, Sun CQ, Wang Z-Y. 2005. BZR1 Is a transcriptional repressor with dual roles in Brassinosteroid homeostasis and growth responses. *Science* **307**: 1634–1638.

He Y, Zhao Y, Hu J, Wang L, Li L, Zhang X, Zhou Z, Chen L, Wang H, Wang J *et al.* 2024. The OsBZR1–OsSPX1/2 module fine-tunes the growth–immunity trade-off in adaptation to phosphate availability in rice. *Molecular Plant* **17**: 258–276.

Hinckley E-LS, Crawford JT, Fakhraei H, Driscoll CT. 2020. A shift in sulfur-cycle manipulation from atmospheric emissions to agricultural additions. *Nature Geoscience* **13**: 597–604.

Hirai MY, Fujiwara T, Chino M, Naito S. 1995. Effects of sulfate concentrations on the expression of a soybean seed storage protein gene and its reversibility in transgenic *Arabidopsis thaliana*. *Plant and Cell Physiology* **36**: 1331–1339.

Jia M, Chen X, Shi X, Fang Y, Gu Y. 2023. Nuclear transport receptor KA120 regulates molecular condensation of MAC3 to coordinate plant immune activation. *Cell Host & Microbe* **31**: 1685–1699.

Jores T, Tonnies J, Wrightsman T, Buckler ES, Cuperus JT, Fields S, Queitsch C. 2021. Synthetic promoter designs enabled by a comprehensive analysis of plant core promoters. *Nature Plants* **7**: 842–855.

Kataoka T, Hayashi N, Yamaya T, Takahashi H. 2004a. Root-to-shoot transport of sulfate in Arabidopsis. Evidence for the role of SULTR3;5 as a component of low-affinity sulfate transport system in the root vasculature. *Plant Physiology* **136**: 4198–4204.

Kataoka T, Watanabe-Takahashi A, Hayashi N, Ohnishi M, Mimura T, Buchner P, Hawkesford MJ, Yamaya T, Takahashi H. 2004b. Vacuolar sulfate transporters are essential determinants controlling internal distribution of sulfate in Arabidopsis. *Plant Cell* **16**: 2693–2704.

Kim E-J, Lee S-H, Park C-H, Kim S-H, Hsu C-C, Xu S, Wang Z-Y, Kim S-K, Kim T-W. 2019. Plant U-Box40 mediates degradation of the Brassinosteroid-responsive transcription factor BZR1 in Arabidopsis roots. *Plant Cell* **31**: 791–808.

Kim T-W, Guan S, Sun Y, Deng Z, Tang W, Shang J-X, Sun Y, Burlingame AL, Wang Z-Y. 2009. Brassinosteroid signal transduction from cell-surface receptor kinases to nuclear transcription factors. *Nature Cell Biology* **11**: 1254–1260.

Lee B-R, Koprivova A, Kopriva S. 2011. The key enzyme of sulfate assimilation, adenosine 5′-phosphosulfate reductase, is regulated by HY5 in Arabidopsis. *The Plant Journal* **67**: 1042–1054.

Lee S-H, Kim S-H, Park T-K, Kim Y-P, Lee J-W, Kim T-W. 2024. Transcription factors BZR1 and PAP1 cooperate to promote anthocyanin biosynthesis in Arabidopsis shoots. *Plant Cell* **36**: 3654–3673.

Li J, Chory J. 1997. A putative leucine-rich repeat receptor kinase involved in Brassinosteroid signal transduction. *Cell* **90**: 929–938.

Li J, Nam KH. 2002. Regulation of Brassinosteroid signaling by a GSK3/SHAGGY-like kinase. *Science* **295**: 1299–1301.

Li J, Wen J, Lease K, Doke J, Tax F, Walker J. 2002. BAK1, an Arabidopsis LRR receptor-like protein kinase, interacts with BRI1 and modulates brassinosteroid signaling. *Cell* **110**: 213–222.

Liang T, Mei S, Shi C, Yang Y, Peng Y, Ma L, Wang F, Li X, Huang X, Yin Y *et al.* 2018. UVR8 interacts with BES1 and BIM1 to regulate transcription and photomorphogenesis in Arabidopsis. *Developmental Cell* **44**: 512–523.

Liu X, Zhu JK, Zhao C. 2023. Liquid-liquid phase separation as a major mechanism of plant abiotic stress sensing and responses. *Stress Biology* **3**: 56.

Mahendrawada L, Warfield L, Donczew R, Hahn S. 2025. Low overlap of transcription factor DNA binding and regulatory targets. *Nature* **642**: 796–804.

Maruyama-Nakashita A, Nakamura Y, Tohge T, Saito K, Takahashi H. 2006. Arabidopsis SLIM1 is a central transcriptional regulator of plant sulfur response and metabolism. *Plant Cell* **18**: 3235–3251.

Nam KH, Li J. 2002. BRI1/BAK1, a receptor kinase pair mediating Brassinosteroid signaling. *Cell* **110**: 203–212.

Nolan T, Liu S, Guo H, Li L, Schnable P, Yin Y. 2017. Identification of Brassinosteroid target genes by chromatin immunoprecipitation followed by high-throughput sequencing (ChIP-seq) and RNA-sequencing. In: Russinova E, Caño-Delgado AI, eds. *Brassinosteroids: methods and protocols*. Springer New York: New York, NY, USA, 63–79.

Nolan TM, Vukašinović N, Liu D, Russinova E, Yin Y. 2020. Brassinosteroids: multidimensional regulators of plant growth, development, and stress responses. *Plant Cell* **32**: 295–318.

Nosaki S, Miyakawa T, Xu Y, Nakamura A, Hirabayashi K, Asami T, Nakano T, Tanokura M. 2018. Structural basis for brassinosteroid response by BIL1/BZR1. *Nature Plants* **4**: 771–776.

Oh E, J-Y Z, M-Y B, RA A, Y S, Z-Y W. 2014. Cell elongation is regulated through a central circuit of interacting transcription factors in the Arabidopsis hypocotyl. *eLife* **3**: e03031.

Oh E, Zhu J-Y, Wang Z-Y. 2012. Interaction between BZR1 and PIF4 integrates brassinosteroid and environmental responses. *Nature Cell Biology* **14**: 802–809.

Pettersen EF, Goddard TD, Huang CC, Meng EC, Couch GS, Croll TI, Morris JH, Ferrin TE. 2021. UCSF ChimeraX: structure visualization for researchers, educators, and developers. *Protein Science* **30**: 70–82.

Planas-Riverola A, Gupta A, Betegón-Putze I, Bosch N, Ibañes M, Caño-Delgado AI. 2019. Brassinosteroid signaling in plant development and adaptation to stress. *Development* **146**: dev151894.

Ristova D, Kopriva S. 2022. Sulfur signaling and starvation response in Arabidopsis. *IScience* **25**: 104242.

Russinova E, Borst J-W, Kwaaitaal M, Caño-Delgado A, Yin Y, Chory J, de Vries SC. 2004. Heterodimerization and endocytosis of Arabidopsis Brassinosteroid receptors BRI1 and AtSERK3 (BAK1). *Plant Cell* **16**: 3216–3229.

She J, Han Z, Kim T-W, Wang J, Cheng W, Chang J, Shi S, Wang J, Yang M, Wang Z-Y *et al.* 2011. Structural insight into brassinosteroid perception by BRI1. *Nature* **474**: 472–476.

Shibagaki N, Grossman AR. 2006. The role of the STAS domain in the function and biogenesis of a sulfate transporter as probed by random mutagenesis. *Journal of Biological Chemistry* **281**: 22964–22973.

Singh AP, Fridman Y, Friedlander-Shani L, Tarkowska D, Strnad M, Savaldi-Goldstein S. 2014. Activity of the Brassinosteroid transcription factors BRASSINAZOLE RESISTANT1 and BRASSINOSTEROID INSENSITIVE1-ETHYL METHANESULFONATE-SUPPRESSOR1/BRASSINAZOLE RESISTANT2 blocks developmental reprogramming in response to low phosphate availability. *Plant Physiology* **166**: 678–688.

Spoel SH, Mou Z, Tada Y, Spivey NW, Genschik P, Dong X. 2009. Proteasome-mediated turnover of the transcription coactivator NPR1 plays dual roles in regulating plant immunity. *Cell* **137**: 860–872.

Sun Y, Fan X-Y, Cao D-M, Tang W, He K, Zhu J-Y, He J-X, Bai M-Y, Zhu S, Oh E *et al.* 2010. Integration of Brassinosteroid signal transduction with the transcription network for plant growth regulation in Arabidopsis. *Developmental Cell* **19**: 765–777.

Tabatabai MA. 1974. A rapid method for determination of sulfate in water samples. *Environmental Letters* **7**: 237–243.

Takahashi H. 2019. Sulfate transport systems in plants: functional diversity and molecular mechanisms underlying regulatory coordination. *Journal of Experimental Botany* **70**: 4075–4087.

Takahashi H, Watanabe-Takahashi A, Smith FW, Blake-Kalff M, Hawkesford MJ, Saito K. 2000. The roles of three functional sulphate transporters involved in uptake and translocation of sulphate in *Arabidopsis thaliana*. *The Plant Journal* **23**: 171–182.

Tang W, Yuan M, Wang R, Yang Y, Wang C, Oses-Prieto JA, Kim T-W, Zhou H-W, Deng Z, Gampala SS *et al.* 2011. PP2A activates brassinosteroid-responsive gene expression and plant growth by dephosphorylating BZR1. *Nature Cell Biology* **13**: 124–131.

Tian Y, Fan M, Qin Z, Lv H, Wang M, Zhang Z, Zhou W, Zhao N, Li X, Han C *et al.* 2018. Hydrogen peroxide positively regulates brassinosteroid signaling through oxidation of the BRASSINAZOLE-RESISTANT1 transcription factor. *Nature Communications* **9**: 1063.

Unterholzner SJ, Rozhon W, Poppenberger B. 2017. Analysis of In Vitro DNA interactions of Brassinosteroid-controlled transcription factors using electrophoretic mobility shift assay. In: Russinova E, Caño-Delgado AI, eds. *Brassinosteroids: methods and protocols*. Springer New York: New York, NY, USA, 133–144.

Vukašinović N, Wang Y, Vanhoutte I, Fendrych M, Guo B, Kvasnica M, Jiroutová P, Oklestkova J, Strnad M, Russinova E. 2021. Local brassinosteroid biosynthesis enables optimal root growth. *Nature Plants* **7**: 619–632.

Wang M, Cai C, Li Y, Tao H, Meng F, Sun B, Miao H, Wang Q. 2023. Brassinosteroids fine-tune secondary and primary sulfur metabolism through BZR1-mediated transcriptional regulation. *Journal of Integrative Plant Biology* **65**: 1153–1169.

Wang R, Wang R, Liu M, Yuan W, Zhao Z, Liu X, Peng Y, Yang X, Sun Y, Tang W. 2021. Nucleocytoplasmic trafficking and turnover mechanisms of BRASSINAZOLE RESISTANT1 in Arabidopsis thaliana. *Proceedings of the National Academy of Sciences, USA* **118**: e2101838118.

Wang T, Chen X, Ju C, Wang C. 2023a. Calcium signaling in plant mineral nutrition: from uptake to transport. *Plant Communications* **4**: 100678.

Wang T, Li M, Yang J, Li M, Zhang Z, Gao H, Wang C, Tian H. 2023b. Brassinosteroid transcription factor BES1 modulates nitrate deficiency by promoting NRT2.1 and NRT2.2 transcription in Arabidopsis. *The Plant Journal* **114**: 1443–1457.

Wang T, Wang P, Theys N, Tong D, Hendrick F, Zhang Q, Van Roozendael M. 2018. Spatial and temporal changes in SO_2 regimes over China in the recent decade and the driving mechanism. *Atmospheric Chemistry and Physics* **18**: 18063–18078.

Wang X, Kota U, He K, Blackburn K, Li J, Goshe MB, Huber SC, Clouse SD. 2008. Sequential transphosphorylation of the BRI1/BAK1 receptor kinase complex impacts early events in brassinosteroid signaling. *Developmental Cell* **15**: 220–235.

Wang Z-Y, Nakano T, Gendron J, He J, Chen M, Vafeados D, Yang Y, Fujioka S, Yoshida S, Asami T *et al.* 2002. Nuclear-localized BZR1 mediates brassinosteroid-induced growth and feedback suppression of brassinosteroid biosynthesis. *Developmental Cell* **2**: 505–513.

Wawrzyńska A, Sirko A. 2020. Proteasomal degradation of proteins is important for the proper transcriptional response to sulfur deficiency conditions in plants. *Plant and Cell Physiology* **61**: 1548–1564.

Xu W, Huang J, Li B, Li J, Wang Y. 2008. Is kinase activity essential for biological functions of BRI1? *Cell Research* **18**: 472–478.

Xu Z-R, Cai M-L, Chen S-H, Huang X-Y, Zhao F-J, Wang P. 2021. High-affinity sulfate transporter Sultr1;2 is a major transporter for Cr(VI) uptake in plants. *Environmental Science & Technology* **55**: 1576–1584.

Yan Z, Zhao J, Peng P, Chihara RK, Li J. 2009. BIN2 functions redundantly with other Arabidopsis GSK3-like kinases to regulate brassinosteroid signaling. *Plant Physiology* **150**: 710–721.

Yao X, Li Y, Chen J, Zhou Z, Wen Y, Fang K, Yang F, Li T, Zhang D, Lin H. 2022. Brassinosteroids enhance BES1-required thermomemory in *Arabidopsis thaliana*. *Plant, Cell & Environment* **45**: 3492–3504.

Yin Y, Vafeados D, Tao Y, Yoshida S, Asami T, Chory J. 2005. A new class of transcription factors mediates brassinosteroid-regulated gene expression in Arabidopsis. *Cell* **120**: 249–259.

Yin Y, Wang Z-Y, Mora-Garcia S, Li J, Yoshida S, Asami T, Chory J. 2002. BES1 accumulates in the nucleus in response to brassinosteroids to regulate gene expression and promote stem elongation. *Cell* **109**: 181–191.

Yoshimoto N, Inoue E, Saito K, Yamaya T, Takahashi H. 2003. Phloem-localizing sulfate transporter, Sultr1;3, mediates re-distribution of sulfur from source to sink organs in Arabidopsis. *Plant Physiology* **131**: 1511–1517.

Yoshimoto N, Inoue E, Watanabe-Takahashi A, Saito K, Takahashi H. 2007. Posttranscriptional regulation of high-affinity sulfate transporters in Arabidopsis by sulfur nutrition. *Plant Physiology* **145**: 378–388.

Yoshimoto N, Takahashi H, Smith FW, Yamaya T, Saito K. 2002. Two distinct high-affinity sulfate transporters with different inducibilities mediate uptake of sulfate in Arabidopsis roots. *The Plant Journal* **29**: 465–473.

Yu X, Li L, Zola J, Aluru M, Ye H, Foudree A, Guo H, Anderson S, Aluru S, Liu P *et al.* 2011. A brassinosteroid transcriptional network revealed by genome-wide identification of BESI target genes in *Arabidopsis thaliana*. *The Plant Journal* **65**: 634–646.

Yu Y, Zhong Z, Ma L, Xiang C, Chen J, Huang X-Y, Xu P, Xiong Y. 2022. Sulfate-TOR signaling controls transcriptional reprogramming for shoot apex activation. *New Phytologist* **236**: 1326–1338.

Zhang H, Liu Y, Zhang X, Ji W, Kang Z. 2023. A necessary considering factor for breeding: growth-defense tradeoff in plants. *Stress Biology* **3**: 6.

Zhou Z, Tran PQ, Cowley ES, Trembath-Reichert E, Anantharaman K. 2025. Diversity and ecology of microbial sulfur metabolism. *Nature Reviews Microbiology* **23**: 122–140.

Zhu T, Wei C, Yu Y, Zhang Z, Zhu J, Liang Z, Song X, Fu W, Cui Y, Wang Z-Y *et al.* 2024. The BAS chromatin remodeler determines brassinosteroid-induced transcriptional activation and plant growth in Arabidopsis. *Developmental Cell* **59**: 924–939.

Supporting Information

Additional Supporting Information may be found online in the Supporting Information section at the end of the article.

Fig. S1 Establishment of S deficiency condition.

Fig. S2 BR biosynthesis genes were upregulated under S deficiency condition.

Fig. S3 BZR1 and BES1 mediate BR signaling-regulated response to S deficiency.

Fig. S4 Phenotypic analysis of *BZR1-/BES1*-related lines under S deficiency condition.

Fig. S5 Expression analysis of *BZR1* and *BES1* and their homologs.

Fig. S6 BES1 activates the expression of *SULTR1*;*2*.

Fig. S7 AlphaFold3 predictions show the interaction between BZR1 DNA-binding domain and DNA fragment on *SULTR1*;*2* promoter.

Fig. S8 Expression of *SULTR1*;*2* in *bzr1-1D*/*sultr1*;*2* mutant.

Fig. S9 The response of S deficiency is BR dependent.

Fig. S10 BZR1 positively regulates sulfate uptake through *SULTR1*;*2*.

Fig. S11 BZR1 promotes anthocyanin accumulation under S deficiency conditions.

Fig. S12 Sulfate content in *bri1-301* and *bin2-3 bil1 bil2* under S deficiency conditions.

Table S1 Primers used in this study.

Please note: Wiley is not responsible for the content or functionality of any Supporting Information supplied by the authors. Any queries (other than missing material) should be directed to the *New Phytologist* Central Office.